Journal of Engineering and Applied Sciences 12 (8): 2220-2228, 2017
ISSN: 1816-949X

Investigating the Radiation Models on the Triangular Collector

[1]Hamid Baghnovi and [2]Taha Talebian
[1]Department of Mechanical Engineering,
Neyshabur Branch, Islamic Azad University, Neyshabur, Iran
[2]Department of Mechanical Engineering, Faculty of Engineering,
Neyshabur Branch, Islamic Azad University, Neyshabur, Iran

Abstract: In this study, numerical simulation and investigation of different radiation models on the triangular solar collector have been initially addressed. In this study, the effect of the change in the bottom wall temperature, an apex angle of 40°, the temperature changes of the lateral walls of the triangle, various types of radiation models in the steady and transient states and also the impact of changes in the Grash of number, Nusselt number and heat transfer coefficient on the performance of the collector and contours of temperature, pressure and speed in the steady state have been investigated. By doing the above activities, the obtained results are listed as follows. In all states, two separate flows are generated inside the chamber as a result of temperature difference between the walls and the bottom surface. Heat transfer coefficient has a minimum value in the middle of the wall. The reason is the existence of the stagnation point and the minimum speed at this point. The amount of heat transfer decreases from the left and right edges towards the middle of the absorbent. Speed changes of the bottom wall of the absorbent reach from a maximum value in both left and right walls to a minimum value in the middle. Pressure also has a maximum amount on both right and left sides and in the middle part which is the stagnation point, we will have a minimal amount of pressure. The heat flux in the transient state is not fixed in the bottom and has a maximum value in the middle and respectively decreases to the left and right walls. The behavior of changes in pressure and speed in the transient state is similar to the steady state. In the transient state, the Nusselt number is reduced from the beginning of the analysis time by increasing the time steps until after 8 sec, the changes of the Nusselt number reach their minimum amount and then, it remains constant. In the transient state, static and dynamic pressures and speed rate increase with the increasing of the time step.

Key words: Heat transfer, nusselt number, grashof number, solar collector, radiation models, numerical solution

INTRODUCTION

Oil shocks of the 70's and the risk of exhaustible fossil energy sources and also nuclear power plant emissions have led humans to new sources of energy that do not have the problems of the mentioned sources. Sun is a major source of energy that can be used as a useful resource and energy supplier in most parts of the world. Many studies have been conducted in recent years on the conversion of solar energy into electrical or thermal energy or both which reflects the importance of this issue (Rahman *et al*., 2012). Besides, the widespread and increasing use of refrigeration industry, springhouse, massive and commercial towers for summer air conditioning, small food industry to huge oil and gas and petrochemical industries for evaporation and distillation and separation refer to the necessity of using the alternative energy. The solar collectors can be applied for the required heat, cooling and heating systems, heating the intended spaces and drying agricultural, textile and marine products.

In 1880, the first flat solar collector was built by Charles Taylor. In the 19th century, solar desalination devices became fashionable. Further, on 22 November 2012, the first completely Iranian solar collector was put into operation in Shiraz solar power plant. A drip water collector was built and installed for the first time on a house roof in Maryland by Harry Thompson in 1959 (Rahman *et al*., 2014a, b). Also, in 2015, Chen and his colleagues introduced and studied heat pipe combined photovoltaic solar collector system. A new type of two-user solar collector in the form of tiles was proposed by Liu solar collector which uses a combination of water and air as the working fluid was provided by Jeremy. A number of factors to be considered in the design of these collectors are as follows:

Corresponding Author: Hamid Baghnovi, Department of Mechanical Engineering, Neyshabur Branch, Islamic Azad University, Neyshabur, Iran

- Thermal performance
- Cost
- Lifespan, durability or sustainability, ease of installation and commissioning

Solar systems can be broadly classified into the following five groups:

- Photobiological systems
- Photochemical systems
- PV systems
- Thermal systems
- Photovoltaic-thermal systems

But different kinds of collectors are Yang and Zuo (2015):

- Flat plate collectors
- Concentrating collectors
- Non-concentrating collectors

Among the non-power applications of solar thermal systems, the following can be mentioned:

- Passive solar heating system (Currie, 2002)
- Active solar heating system (Tokit *et al*., 2013)
- Solar cooling system (Suman *et al*., 2015)
- Solar powered desalination unit (Tian and Zhao, 2013)
- Solar cooker (Yuan *et al*., 2011)

Extraction of equations: The results obtained from the numerical solution include less cost and time compared to analytical and laboratory solutions. Given that we had to use several stages of replications to achieve the optimal conditions in laboratory works, this method will cost a lot. Also, due to the relative complexity of partial differential equations governing the sample, analytical solutions provided are accompanied by numerous assumptions that reduce the accuracy of the results.

Continuity equation: The principle of mass conservation states that mass is neither produced nor destroyed and this principle is expressed by the continuity equation (Tokit *et al*., 2013) for compressible fluids:

$$\frac{\partial \rho}{\partial t} + \vec{\nabla}.(\rho\vec{V}) = 0$$

For incompressible fluids:

$$(\vec{\nabla}.\vec{V}) = 0$$

Where:
V = The velocity vector
ρ = Density
t = The time

Momentum equation: Fluid mechanics is not specified only by having the continuity equation but the principle of conservation of momentum or Newton's second law should be stated about it. Considering the incompressible flow and assuming the coefficient of viscosity as fixed, the Navier-Stokes equation is as follows (Yang and Zuo, 2015):

$$\frac{D\rho}{Dt} = \rho f - \nabla P + \mu\nabla^2 V$$

Where:
V = The velocity vector
P = The pressure
f = Volumetric forces
μ = The viscosity.
D/Dt = The material derivative which is defined as:

$$\left(\frac{D\varphi}{Dt} = \frac{\partial \varphi}{\partial x} + \vec{V}, \nabla\varphi\right)$$

Assuming the constant viscosity and regardless of volumetric forces, Navier-Stokes equations are simplified as follows (Tian and Zhao, 2013):

$$\frac{\partial(\rho u)}{\partial t} + u\frac{\partial(\rho u)}{\partial x} + v\frac{\partial(\rho u)}{\partial y} + \rho u\frac{\partial u}{\partial x} + \rho u\frac{\partial v}{\partial y} = -\frac{\partial p}{\partial x} + \mu\left(\frac{\partial^2 u}{\partial x^2} + \frac{\partial^2 u}{\partial y^2}\right)$$

$$\frac{\partial(\rho v)}{\partial t} + u\frac{\partial(\rho v)}{\partial x} + v\frac{\partial(\rho v)}{\partial y} + \rho u\frac{\partial v}{\partial x} + \rho u\frac{\partial v}{\partial y} = -\frac{\partial p}{\partial y} + \mu\left(\frac{\partial^2 v}{\partial x^2} + \frac{\partial^2 v}{\partial y^2}\right)$$

Energy equation: According to the conservation of energy principle, the sum of input and produced energy is equal to the sum of output and stored energy in the control volume. Given the insignificance of the term of energy collapse and constant conductivity coefficient, conservation of energy is obtained as follows (Currie, 2002):

$$C_p\left(\frac{\partial(\rho T)}{\partial t} + u\frac{\partial(\rho T)}{\partial x} + v\frac{\partial(\rho T)}{\partial y} + \rho T\frac{\partial u}{\partial x} + \rho T\frac{\partial v}{\partial y}\right) = k\left(\frac{\partial^2 T}{\partial x} + \frac{\partial^2 T}{\partial y}\right)$$

Where:
V = The velocity vector
ρ = Density
t = The time

Mass conservation equations, Navier-Stokes and the energy for transient heat transfer of the geometry expressed are as follows:

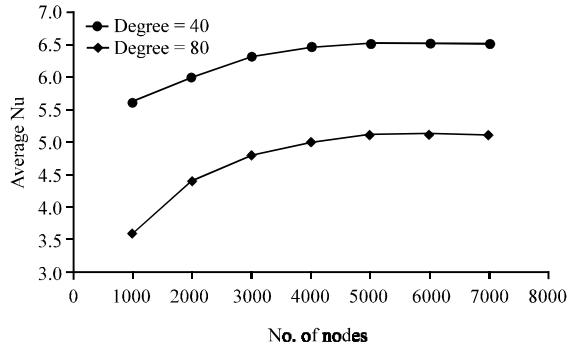

Fig. 1: Network independence

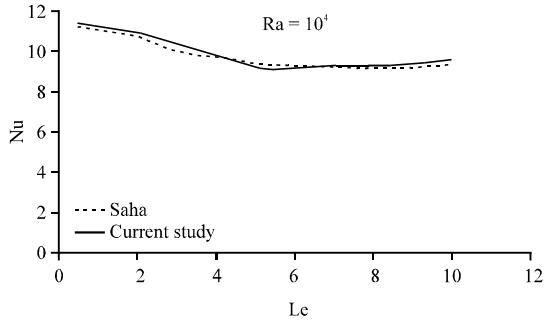

Fig. 2: Validation of the present numerical solution with reference

$$\frac{\partial u}{\partial x}+\frac{\partial v}{\partial y}=0$$

$$\frac{\partial u}{\partial t}+u\frac{\partial u}{\partial x}+v\frac{\partial u}{\partial y}=-\frac{1}{\rho}\frac{\partial p}{\partial x}+\frac{\mu}{\rho}\left(\frac{\partial^2 u}{\partial x^2}+\frac{\partial^2 u}{\partial y^2}\right)$$

$$\frac{\partial v}{\partial t}+u\frac{\partial u}{\partial x}+v\frac{\partial u}{\partial y}=-\frac{1}{\rho}\frac{\partial p}{\partial x}+\frac{\mu}{\rho}\left(\frac{\partial^2 v}{\partial x^2}+\frac{\partial^2 v}{\partial y^2}\right)+\frac{\rho\beta}{\rho}(T-T_c)$$

$$\frac{\partial T}{\partial t}+u\frac{\partial T}{\partial t}+v\frac{\partial T}{\partial y}=\alpha\left(\frac{\partial^2 T}{\partial x^2}+\frac{\partial^2 T}{\partial y^2}\right)$$

Where:

u and v = Respectively the horizontal and vertical components of speed

β = The coefficient of thermal expansion

T_c = The temperature of the collector wall

Dimensionless boundary and initial conditions for the difficulties ahead are as follows: t = 0: u = v = 0, T = Tc; t >0: u = v = 0, T = Th; u = v = 0, T = Tc.

Network independence and validation of the present numerical solution: Figure 1, 40 and 80° of change in the Nusselt number have been displayed for different networks and angles of the collector head. At the end, the network with 5701 nodes was selected as the number of fine mesh for analyses.

Nusselt changes based on the Lewis number obtained from the present numerical model along with the data of Saha and colleagues in the reference (Al-Soud *et al*., 2010) have been shown in Fig. 2. As can be observed, there is good agreement between the results of Saha and colleagues with the present numerical model.

Thermo-physical properties, initial and boundary conditions for problem-solving, hypotheses and geometry of the studied problem: In the simulation of triangular solar collector, lateral walls are made of glass and thermo-physical properties of glass have been stated in Table 1. Moreover, initial and boundary conditions of the problem have been mentioned in Table 2. Hypotheses include; striped horizontal plate of the bottom is of the concentrating collector type and acts as an adsorbent. Temperature of the sloping walls and the bottom wall is variable. The variable temperature of the bottom wall is higher than the variable temperature of the sloping walls. L is the horizontal length and H is the vertical length. The speed in the entire walls is zero. The base temperatures of the lateral walls and the bottom wall of the collector are considered at first to be respectively 310 and 350° Kelvin. Then, these temperatures increase in order to evaluate the effect of temperature changes. Type of the heat transfer is radiation-radioactive and natural convection. Heat transfer finally reaches equilibrium which here, the problem is solved in return for equilibrium (steady) and non-equilibrium (transient) states (Fig. 3).

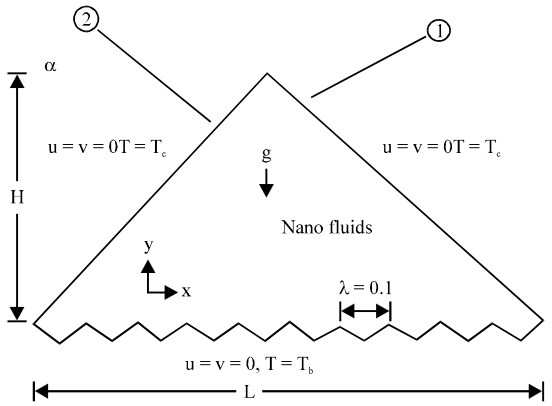

Fig. 3: Geometry of the problem under study

Table 1: Thermo-physical properties of glass

Quantity	Values
Density (kg/m^3)	2500
Specific heat at constant pressure (j/kg-k)	800
Thermal conductivity (w/m-k)	0.8

Table 2: Initial and boundary conditions of the problem

Parameters	Values
Solution timescales (s)	0-9
Type of solution	Steady-transient
The fluid under study	Air
Temperature at the beginning of the Triangle walls (Tc)	310°K
Temperature at the beginning of the Triangle bottom (Th)	350°K
Temperature at the beginning of the base for 22 states	30°K

MATERIALS AND METHODS

Types of radiation models, familiarity with them and examination of them in the steady state: There are five different radiation models in Fluent software which include:

- Discrete Ordinate Model (DOM)
- Discrete Transfer Radiation Model (DTRM)
- P1 Radiation Model
- Rosseland Model
- Surface-to-Surface (S2S)

Discrete classification radiation model (DOM): The method of discrete classification solves the radiation transport equation for a limited number of spatial angles. Unlike the discrete transfer model, the discrete classification model does not act as beam tracking. This model transfers the radiation transport equation to specific coordinates (x, y, z) and solves it. This model comes with surface to surface radiation heat transfer and also includes heat transfer in the semi-transparent medium. This model solves the radiative transfer equation for a limited number of three dimensional discrete angles. Each of these angles is displayed with a direction ($\vec{s}$) which has become fixed in the global Cartesian system. The equation of this model is as follows:

$$\nabla.(I(\vec{r},\vec{s})\vec{s}) + (\alpha+\sigma_s)I(\vec{r},\vec{s}) = \alpha n^2\frac{\sigma T^4}{\pi} + \frac{\sigma_s}{4\pi}\int_0^{4\pi} I(\vec{r},\vec{s}').\phi(\vec{r},\vec{s}').d\Omega'$$

Where:

r = The position vector
s = The direction vector of diffusion
a = The absorption coefficient
σ_s = The diffusion coefficient
σ = Stefan-Boltzmann constant
T = The temperature
n = The refractive index and $(\alpha+\sigma_s)I(\vec{r},\vec{s})$ is the optical thickness of the medium

P1 radiation model: P-1 model is more applicable than the discrete transfer radiation model. In the P-1 method, radiation transport equation is a diffusion equation and a computer with a weaker processing unit is required to solve it. This model also includes diffusion effects and can easily be used for complex models. This model predicts radiative heat fluxes from the local thermal springs or wells. P1 model based on the emission of the radiation intensity I is in the form of spherical harmonic radiations perpendicular to each other. This equation is as follows (Yang and Zuo, 2015):

$$\nabla.\left(\frac{1}{3\alpha+(3-C)\sigma_s}\nabla G\right) + (4\sigma T^4 - G) = 0$$

Rosseland radiation model: Rosseland radiation model or radiation diffuse approximation is used when the medium is optically thick. This procedure gives good results for the problems with the optical thickness >3. The model is derived from the P1 model equations while considering approximations and their difference is that in Rosseland model, it is assumed that the radiation intensity is equal to the intensity of black body radiation at the gas temperature. While in the P1 model, calculations are done on the transport equation, Rosseland model like the P1 model also considers the diffusion effect (Currie, 2002).

Discrete Transfer Radiation Model (DTRM): The basic premise used in the discrete transfer radiation model is that the radiation emitted from the surface elements in a specific range of spatial angles can be approximated by a beam. In this method, it is assumed that all surfaces are diffuse. In other words, reflection of the incoming radiation homogeneously occurs in all directions. The diffusion effect is not considered in this model and problem-solving with a lot of beams creates a limitation for the Computer Processing Unit (CPU).

The energy arising from the radiation in the fluid is calculated by the sum of changes in the radiation intensity of the path of each beam that passes the fluid volume element. The technique applied in this model is beam tracking and can predict the radiative heat transfer between surfaces without the calculation of the view factor of surfaces in relation to each other. The accuracy of this method depends on the number of the transmitted beams and computational networking (Al-Soud *et al*., 2010; Esch *et al*., 2012). The radiation equation in this model is as follows:

$$\frac{dI}{ds} + \alpha I = \alpha\frac{\sigma T^4}{\pi}$$

Where, I is the intensity of radiation. By integrating the above equation, we will have (Kumar and Rosen, 2011):

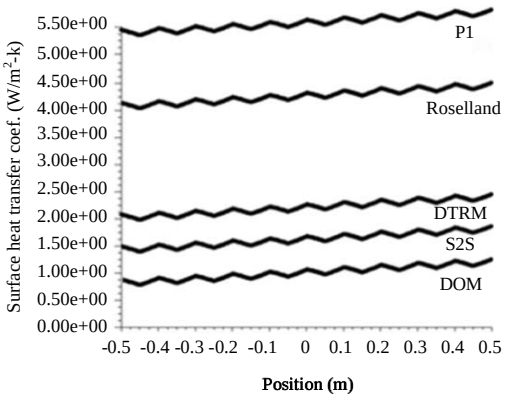

Fig. 4: Changes in the heat transfer coefficient on the bottom wall (with the apex angle of 40°)

$$I(s) = \frac{\sigma T^4}{\pi}(1 - \exp(-as)) + I_0 \exp(as)$$

Surface to Surface radiation model (S2S): This method involves dividing the area of solution into surface areas with the same temperature. The overall energy balance for each area is written based on the radiation from other areas and then these equations are written in terms of the exchange coefficients which are known as directional flux Surfaces (SS).

Radiative energy transfer between two areas is proportional to their directional flux surface. The net radiant energy exchange between two areas is written which is as follows, for example, for the gas area i and surface area j (Chan *et al*., 2010):

$$Q_i \leftrightarrow j - Gi\vec{S}jEg, i - Gi\overleftarrow{S}jEs, j$$

In the equation above, Eg is the radiative power of the black body with the same temperature as the gas. Gi $(Sj)^{\rightarrow}$ and Gi $(Sj)^{\leftarrow}$ are directional flux surfaces. Energy balance equations are written for each surface and gas area. Therefore, a non-linear system of equations is created which through its solution, the temperature of each area and the rate of heat transfer to each area are calculated. Now, we examine the tables, charts, diagrams and contours drawn from the five radiation models listed with the apex angle of 40° (Fig. 4).

As can be seen, P1 model reports the highest rate of heat transfer coefficient and DOM model reports the lowest heat transfer coefficient. And changes from the beginning of the second wall to the first wall have downward and upward trends in multiple intervals. Also, changes are irregular but in the end, the end point compared to the start point has almost an upward trend. As can be observed, by increasing the temperature of the bottom wall, the heat transfer coefficient and

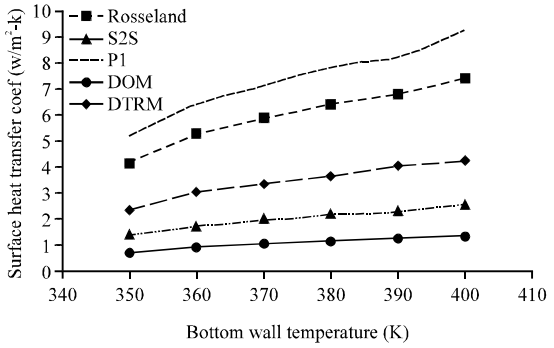

Fig. 5: Changes in the heat transfer coefficient compared to the changes in the temperature of the bottom wall (with the apex angle of 40°)

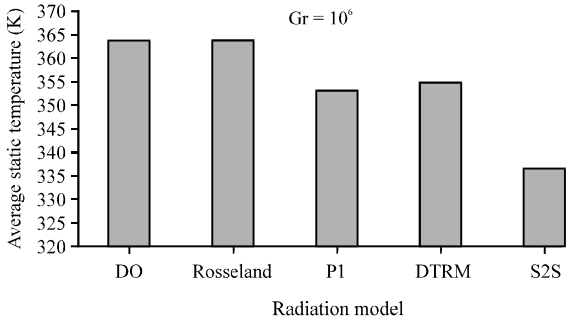

Fig. 6: Average static temperature of the fluid for different models (with the apex angle of 40°)

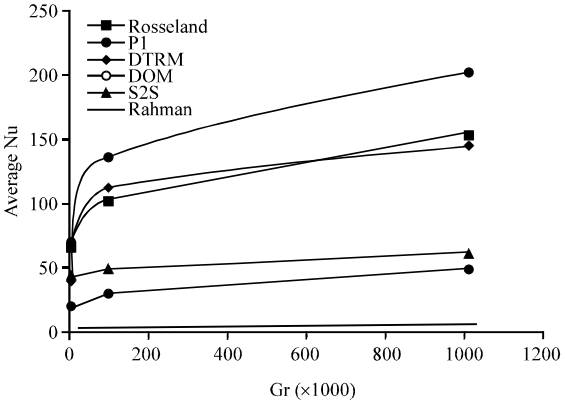

Fig. 7: Average Nusselt changes based on the Grashof number (with the apex angle of 40°)

consequently the rate of heat transfer increase and it has an upward trend. Besides, it can be seen in this Fig. 5 that P1 model estimates the highest heat transfer coefficient and DOM model estimates the lowest heat transfer coefficient. As can be seen, S2S model reports the lowest value and DOM model reports the highest average fluid temperature. As can be observed in Fig. 6 and 7, average

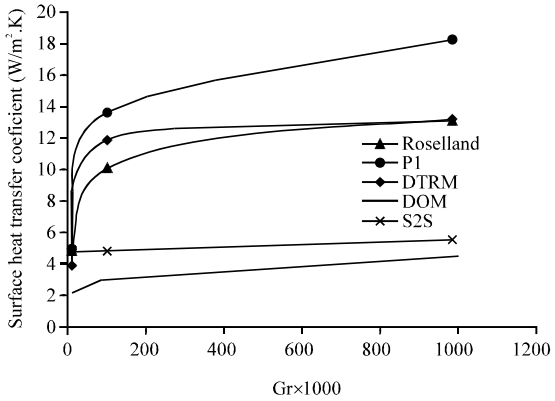

Fig. 8: Changes in the thermal conductivity coefficient based on the Grashof number (with the apex angle of 40°)

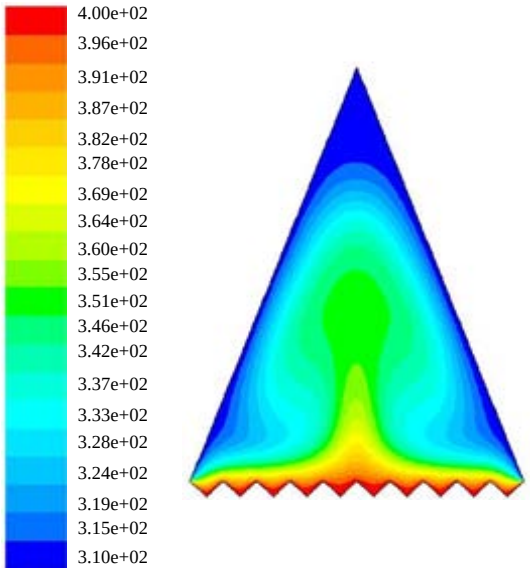

Fig. 9: Static temperature contour for the steady state and apex angle of 40°

Nusselt number and heat transfer coefficient increase with an increase in the Grashof number. The first model, i.e., the DOM model, provides the best answer to solve the problem compared to the work performed by Rahman and colleagues in the reference.

Further, the flow behavior of pressure and temperature contours and flow function for the apex angle of 40° have been shown in the Fig.8-11.

In Fig. 8-11, in all states, two completely separate low-pressure and high-pressure flows are generated inside the chamber as a result of temperature difference between the walls and the bottom surface. The intensity of static temperature distribution is greater in the middle

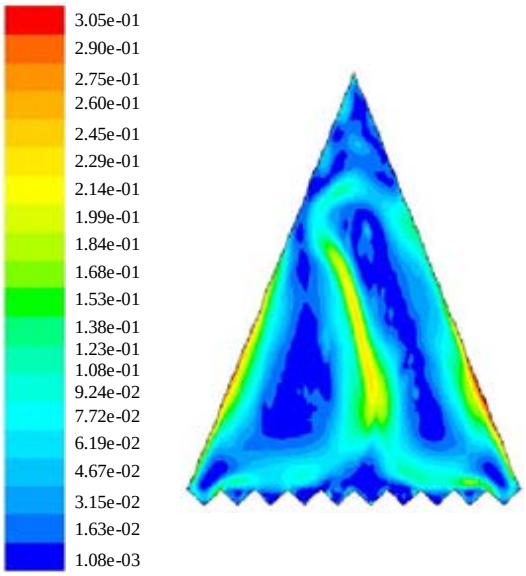

Fig. 10: Dynamic pressure contour for the steady state and apex angle of 40°

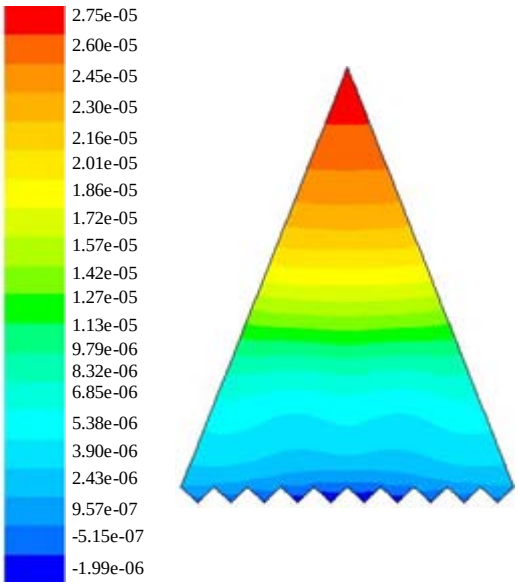

Fig. 11: Static pressure contour for the steady state and apex angle of 40°

of the bottom wall and is reduced by moving towards the sides and vertex of the triangle. The intensity of the dynamic pressure distribution in the middle of the bottom wall and near the triangle's sides is greater than the other parts. The intensity of the static pressure distribution increases by moving from the bottom wall to the triangle vertex.

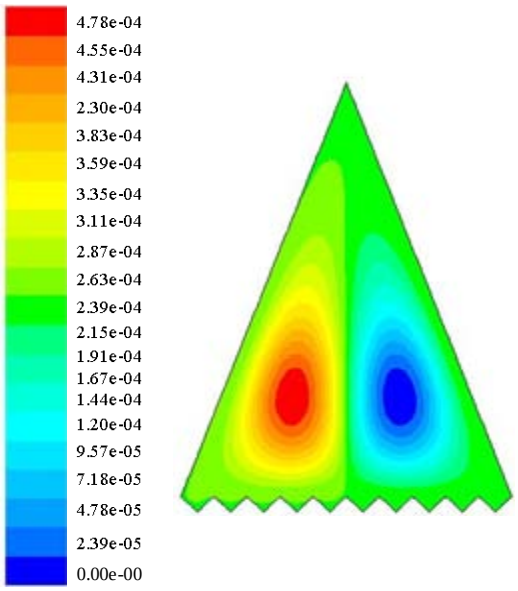

Fig. 12: Flow function contour for the steady state and apex angle of 40°

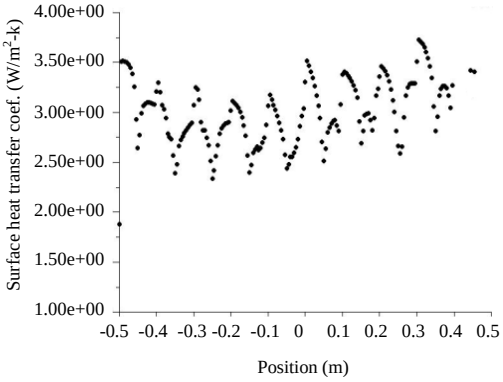

Fig. 13: Changes in the heat transfer coefficient in the bottom wall of the absorbent (with the apex angle of 40° and DOM radiation model); surface heat transfer coef.; ANSYS fluent 15.0 (2d, dp, pbns, lam)

As can be seen in Fig. 12-15, heat transfer coefficient, velocity and pressure have a minimum value at x = 0 or in the middle of the wall. The reason is the existence of the stagnation point and the minimum speed at this point and changes are all irregular.

Investigation of radiation models in the transient state: In Fig. 15 and 16, it can be seen that by increasing the time step, static and dynamic pressures also increase. Additionally, the static pressure has more uniform changes relative to the dynamic pressure. As shown in Fig. 17-18, speed changes are similar to the steady state

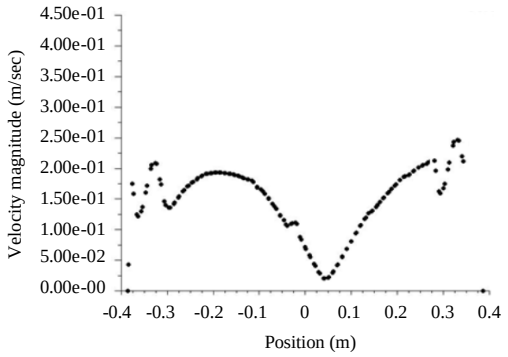

Fig. 14: Speed changes in the bottom wall of the absorbent (with the apex angle of 40° and DOM radiation model); velocity magnitude; ANSYS fluent 15.0 (2d, dp, pbns, lam)

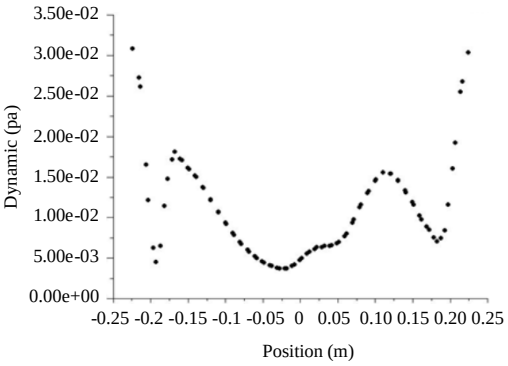

Fig. 15: Dynamic pressure changes in the bottom wall of the absorbent (with the apex angle of 40° and DOM radiation model); dynamic pressure; Apr. 05, 2016 ANSYS fluent 15.0 (2d, dp, pbns, lam)

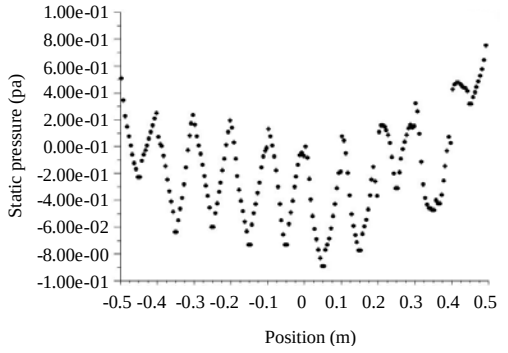

Fig. 16: Static pressure changes in the bottom wall of the absorbent (with the apex angle of 40° and DOM radiation model); static pressure; ANSYS fluent 15.0 (2d, dp, pbns, lam)

and the minimum speed occurs in the middle and the stagnation point. It is also observed that the speed increases with an increase in the time step.

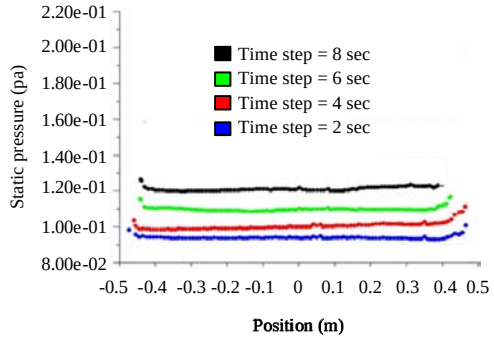

Fig. 17: Static pressure changes in the bottom wall of the absorbent, the transient state with the time steps of 2, 4, 6 and 8 sec (with the apex angle of 40° and DOM radiation model); static pressure (Time = 0.0000e+00); ANSYS fluent 15.0 (2d, dp, pbns, lam, transient)

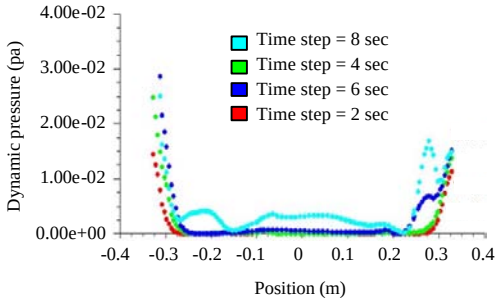

Fig. 18: Dynamic pressure changes in the bottom wall of the absorbent, the transient state with the time steps of 2, 4, 6 and 8 sec (with the apex angle of 40° and DOM radiation model); dynamic pressure (Time = 0.0000e+00); ANSYS fluent 15.0 (2d, dp, pbns, lam, transient)

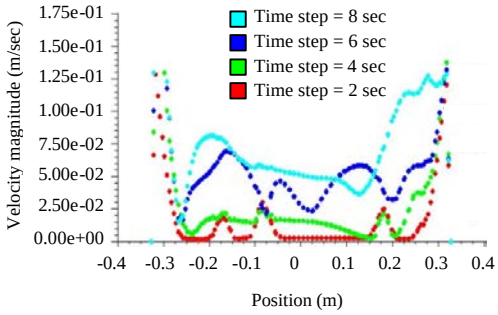

Fig. 19: Speed changes in the bottom wall of the absorbent, the transient state with the time steps of 2, 4, 6 and 8 sec (with the apex angle of 40° and DOM radiation model); static pressure (velocity magnitude Time = 0.0000e+00); ANSYS fluent 15.0 (2d, dp, pbns, lam, transient)

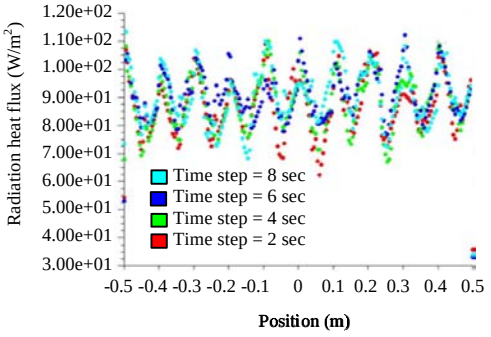

Fig. 20: Bottom heat flux changes, transient state, time steps of 2, 4, 6 and 8 sec (with the apex angle of 40°). It can be seen that the heat flux has a maximum value in the middle unlike the speed and decreases, respectively to the walls of the left and right sides; radiation heat flux (Time = 0.0000e+00); ANSYS fluent 15.0 (2d, dp, pbns, lam, transient)

RESULTS AND DISCUSSION

In all states, two separate flows are generated inside the chamber as a result of temperature difference between the walls and the bottom surface. Heat transfer coefficient has a minimum value in the middle of the wall. The reason is the existence of the stagnation point and the minimum speed at this point. The amount of heat transfer decreases from the left and right edges towards the middle of the absorbent. Speed changes of the bottom wall of the absorbent reach from a maximum value in both left and right walls to a minimum value in the middle. Pressure also has a maximum amount on both right and left sides and in the middle part which is the stagnation point, we will have a minimal amount of pressure. The heat flux in the transient state is not fixed in the bottom and has a maximum value in the middle and respectively decreases to the left and right walls. The behavior of changes in pressure and speed in the transient state is similar to the steady state. In the transient state, the Nusselt number is reduced from the beginning of the analysis time by increasing the time steps until after 8 sec, the changes of the Nusselt number reach their minimum amount and then, it remains constant. In the transient state, static and dynamic pressures and speed rate increase with the increasing of the time step. The intensity of the static temperature distribution is greater in the middle of the bottom wall and is reduced by moving to the sides and vertex of the triangle. The intensity of the dynamic pressure distribution in the middle of the bottom wall and near the triangle's sides is greater than the other parts. The intensity of the static pressure distribution increases by moving from the bottom wall to the triangle vertex.

CONCLUSION

The intensity of the static temperature distribution is greater in the middle of the bottom wall and is reduced by moving to the sides and vertex of the triangle. The intensity of the dynamic pressure distribution in the middle of the bottom wall and near the triangle's sides is greater than the other parts. The intensity of the static pressure distribution increases by moving from the bottom wall to the triangle vertex.

REFERENCES

Al-Soud, M.S., E. Abdallah, A. Akayleh, S. Abdallah and E.S. Hrayshat, 2010. A parabolic solar cooker with automatic two axes sun tracking system. Appl. Energ., 87: 463-470.

Chan, H.Y., S.B. Riffat and J. Zhu, 2010. Review of passive solar heating and cooling technologies. Renew. Sustain. Energy Rev., 14: 781-789.

Currie, I.G., 2002. Fundamental Mechanics of Fluids. 3rd Edn., Taylor and Francis Group, Florida,USA., ISBN:0-8247-2886-5, Pages: 477.

Esch, V.M.M.E., R.H.J. Looman and D.G.J. Bruin-Hordijk, 2012. The effects of urban and building design parameters on solar access to the urban canyon and the potential for direct passive solar heating strategies. Energy Build., 47: 189-200.

Kumar, R. and M.A. Rosen, 2011. A critical review of photovoltaic-thermal solar collectors for air heating. Applied Energy, 88: 3603-3614.

Rahman, M.M., H.F. Oztop, A. Ahsan, M.A. Kalam and Y. Varol, 2012. Double-diffusive natural convection in a triangular solar collector. Int. Commun. Heat Mass Transfer, 39: 264-269.

Rahman, M.M., S. Mojumder, S. Saha, S. Mekhilef and R. Saidur, 2014a. Augmentation of Natural Convection Heat Transfer in Triangular Shape Solar Collector by Utilizing Water Based Nanofluids Having a Corrugated Bottom Wall. Int. Communi. Heat Mass Transfer, 50: 117-127.

Rahman, M.M., S. Saha, S. Mojumder, S. Mekhilef and R. Saidur, 2014b. Numerical Simulation of Unsteady Heat Transfer in a Half Moon Shape Enclosure with Variable Thermal Boundary Condition for Different Nanofluids. Numer. Heat Transfer Part, 65: 282-301.

Suman, S., M.K. Khan and M. Pathak, 2015. Performance enhancement of solar collectors-a review. Renewable Sustainable Energy Rev., 49: 192-210.

Tian, Y. and C.Y. Zhao, 2013. A review of solar collectors and thermal energy storage in solar thermal applications. Appl. Energy, 104: 538-553.

Tokit, E.M., M.Z. Yusoff and H. Mohammed, 2013. Investigation on nanoparticle velocity in two phase approach. Intl. J. Mechan. Aerosp. Ind. Mechatronic Manuf. Eng., 7: 2037-2043.

Yang, K. and C. Zuo, 2015. A novel multi-layer manifold microchannel cooling system for concentrating photovoltaic cells. Energy Conversion Manage., 89: 214-221.

Yuan, G., Z. Wang, H. Li and X. Li, 2011. Experimental study of a solar desalination system based on humidification: Dehumidification process. Desalin., 277: 92-98.